THEORETICAL & APPLIED MECHANICS LETTERS **2**, 061001 (2012)

Fracturing damage process in dynamic split experiments of a brittle glass

Ning Cui,[1, a)] Linmao Ye,[1, b)] and Kaixin Liu[1,2, c)]

[1)] *LTCS and Department of Mechanics & Aerospace Engineering, College of Engineering, Peking University, Beijing 100871, China*

[2)] *Center for Applied Physics and Technology, Peking University, Beijing 100871, China*

(Received 15 July 2012; accepted 25 September 2012; published online 10 November 2012)

Abstract In this study, the 3-dimensional discrete element method is firstly introduced to explain the fracturing damage process of the dynamic split experiment of a special brittle glass ZnS. The corresponding dynamic split experiment is also performed by using the split Hopkinson pressure bar. Then the numerical results correspond closely to those obtained by experiments, and the fracturing damage mode shows that the sample under high strain rate loading would crack along vertical diameter in the band region between two loading edges, which differs from the static damage mode. Furthermore, by comparing a group of contrast numerical tests, the numerical results prove that loading area upon the top side of samples would influence the fracture mode of dynamic split experiments, which indicates that the narrow loading plane is better. [doi:10.1063/2.1206101]

Keywords discrete element method, dynamic split test, brittle material, crack band

Various brittle materials or quasi-brittle materials are likely to damage under impact loading in many engineering practice. And tensile damage is the primary failure mode of most kinds of brittle materials, partly because its compressive strength is higher than the tensile strength, in contrast to other materials. Recently, many scholars have tried to analyze the failure process and damage mode of brittle materials by both experimental technique and numerical simulations, of which rock and concrete are the most common samples.[1–3]

However, because of the limit of equipments and technique, experiments of the dynamic tensile damage are more complicated and difficult comparing with those of the dynamic compressive damage. The corresponding research achievements are rarely obtained. Moreover, the failure process and damage mode of the dynamic split test of brittle materials are insufficient.

As one of the most famous experimental equipments to solve dynamic impact problems, the split Hopkinson pressure bar (SHPB), which is firstly proposed as a pressure bar by Hopkinson in 1941 and improved by Kolsky in 1949 afterwards,[4] shows its huge advantage to record the dynamic curves of stress-strain, stress-time and strain rate-time by applying the high speed compressive load in laboratory.[5–7] And also SHPB provides possibility of research towards dynamic characters of brittle materials.[8–12] However, few scholars research the dynamic tensile damage process of brittle materials with the help of SHPB.

On the other hand, many traditional continuum-based numerical methods, for instance the finite element method (FEM), to describe and model the damage process of such materials accurately and efficiently, are conducted. Although many of these continuum-based numerical methods have developed dynamical package to adapt the requirement of damage process, there are still a great number of difficulties in overcoming the algorithm distortion, such as mass losing and frequent re-meshing while damage appears. As a traditional discontinuum-based numerical method, the discrete element method (DEM), which was originally proposed by Cundall and Potyondy,[13] has been developed maturely for solving the complex impact problems, which can apply to not only the behavior of a continuum but also the transformation from a continuum to a discontinuum such as the fracturing damage process of some brittle materials.[14–20]

In this work, efforts are made to clarify the damage process and tensile failure modes of special glass containing ZnS under dynamic load through the dynamic split test. With the requirement of high strain rate, SHPB is introduced to apply the high speed tensile load in this dynamic split test. Then a DEM model is established, and shows the whole damage process from the continuum to the discontinuum of samples. Analyzing the results of experiments and DEM simulations, the dynamic tensile fracture modes of the brittle glass are obtained. In addition, advice on how to narrow the crack band is proposed.

To illustrate the dynamic split test, numerical method such as the discrete element method can be used to simulate the damage progress. As the shape of the disc sample we used, the DEM for 3-D problem conform to the experiment.

As shown in Fig. 1, for a 3-D problem, the sample is constituted by a number of uniform rigid spherical elements. All the elements are linked by three springs that one normal spring k_{n} and two tangential springs k_s, k_m.

We suppose the cylinder sample is subdivided into

[a)] Email: Cuining1988@pku.edu.cn.
[b)] Email: lmleaf001@gmail.com.
[c)] Corresponding author. Email: Kliu@pku.edu.cn.

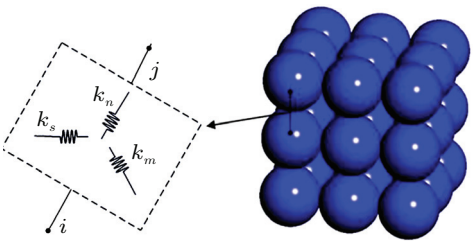

Fig. 1. The discrete element models for 3-D problems.

N sphere elements. And in the sphere-spring model, the deformation effect of an elastic body is expressed by the deformation of springs between elements. Assuming sphere i connects with p spheres nearby, the average strain energy around sphere i can be expressed as follows[19]

$$U_i = \frac{1}{2V_i}\sum_j^p \Big[k_{nij}(u_{nj}-u_{ni})^2 + \frac{1}{2}k_{sij}(u_{sj}-u_{si})^2 + \frac{1}{2}k_{mij}(u_{mj}-u_{mi})^2\Big], \quad (1)$$

where U_i is the average strain energy around sphere i, V_i is the volume of sphere i, k_{nij} is the normal spring constants between spheres i and j, while k_{sij} and k_{mij} are the spring constants between spheres i and j along the two tangential directions, respectively; u_{ni} and u_{si}, u_{mi} are the normal and the tangential displacements of sphere i. u_{nj} and u_{sj}, u_{mj} are the normal and the two tangential displacements of sphere j, respectively.

There are two sets of Cartesian coordinates, one of which is for the global coordinate and the other for the local coordinate. We take sphere i and an arbitrary sphere j that surrounds it into consideration and suppose $l_1 = \cos\alpha$, $l_2 = \cos\beta$ and $m_2 = \sin\beta$, the relationship of relative displacements between the global and the local coordinate can be written as

$$\begin{aligned} u_{ni}-u_{nj} &= l_1l_2(u_{xi}-u_{xj}) + m_2(u_{yi}-u_{yj}) + m_1l_2(u_{zi}-u_{zj}),\\ u_{si}-u_{sj} &= -l_1m_2(u_{xi}-u_{xj}) + l_2(u_{yi}-u_{yj}) - m_1m_2(u_{zi}-u_{zj}),\\ u_{mi}-u_{mj} &= -m_1(u_{xi}-u_{xj}) + l_1(u_{zi}-u_{zj}). \end{aligned} \quad (2)$$

The total potential energy of this sphere-spring system can be described as follows

$$\begin{aligned} \Pi = &\sum_i^N (U_iV_i) + \sum_i^N (u_{xi}\rho\ddot{u}_{xi}V_i + u_{yi}\rho\ddot{u}_{yi}V_i + u_{zi}\rho\ddot{u}_{zi}V_i) - \\ &\sum_i^N (u_{xi}f_{xi}V_i + u_{yi}f_{yi}V_i + u_{zi}f_{zi}V_i) - \\ &\sum_i^N (u_{xi}\bar{T}_{xi}S_i + u_{yi}\bar{T}_{yi}S_i + u_{zi}\bar{T}_{zi}S_i), \end{aligned} \quad (3)$$

where ρ is the mass density of the sample, S_i is the boundary area of external force on sphere i. u_{xi}, u_{yi}, along with u_{zi} are the displacements of sphere i in the x, y, z directions; while $\ddot{u}_{xi}$, $\ddot{u}_{yi}$ and $\ddot{u}_{zi}$ are the displacements accelerations; f_{xi}, f_{yi}, f_{zi} and $\overline{T}_{xi}$, $\overline{T}_{yi}$, $\overline{T}_{zi}$ are the components of body force and surface force on sphere i in the x, y, z directions, respectively.

Substituting Eq. (2) into Eq. (1), then make $\partial\Pi/\partial u_{xi} = 0$, $\partial\Pi/\partial u_{yi} = 0$ and $\partial\Pi/\partial u_{zi} = 0$ in accordance with the variational calculus. The displacements accelerations, $\ddot{u}_{xi}$, $\ddot{u}_{yi}$ and $\ddot{u}_{zi}$, can be obtained as follows

$$\begin{aligned} \ddot{u}_{xi} = \frac{1}{\rho V_i}\Big\{ & f_{xi}V_i + \bar{T}_{xi}S_i + \sum_j^p k_{nij}[l_{ij1}^2l_{ij2}^2(u_{xj}-u_{xi}) + l_{ij1}m_{ij2}l_{ij2}(u_{yj}-u_{yi}) + l_{ij1}l_{ij2}^2m_{ij1}(u_{zj}-u_{zi})] + \\ & \sum_j^p k_{sij}[l_{ij1}^2m_{ij2}^2(u_{xj}-u_{xi}) - l_{ij1}l_{ij2}m_{ij2}(u_{yj}-u_{yi}) + l_{ij1}l_{ij2}m_{ij1}m_{ij2}(u_{zj}-u_{zi})] + \\ & \sum_j^p k_{mij}[m_{ij1}^2(u_{xj}-u_{xi}) - m_{ij1}l_{ij1}(u_{zj}-u_{zi})]\Big\}, \\ \ddot{u}_{yi} = \frac{1}{\rho V_i}\Big\{ & f_{xi}V_i + \bar{T}_{xi}S_i + \sum_j^p k_{nij}[l_{ij1}l_{ij2}m_{ij2}(u_{xj}-u_{xi}) + m_{ij2}^2(u_{yj}-u_{yi}) + l_{ij2}m_{ij1}m_{ij2}(u_{zj}-u_{zi})] + \\ & \sum_j^p k_{sij}[-l_{ij1}m_{ij2}l_{ij2}(u_{xj}-u_{xi}) + l_{ij2}^2(u_{yj}-u_{yi}) - l_{ij2}m_{ij1}m_{ij2}(u_{zj}-u_{zi})]\Big\}, \\ \ddot{u}_{zi} = \frac{1}{\rho V_i}\Big\{ & f_{xi}V_i + \bar{T}_{xi}S_i + \sum_j^p k_{nij}[l_{ij1}l_{ij2}^2m_{ij1}(u_{xj}-u_{xi}) + m_{ij1}l_{ij2}m_{ij2}(u_{yj}-u_{yi}) + l_{ij2}^2m_{ij1}^2(u_{zj}-u_{zi})] + \\ & \sum_j^p k_{sij}[l_{ij1}l_{ij2}m_{ij1}m_{ij2}(u_{xj}-u_{xi}) - l_{ij2}m_{ij1}m_{ij2}(u_{yj}-u_{yi}) + \end{aligned}$$

$$m_{ij1}^2 m_{ij2}^2 (u_{zj} - u_{zi})] + \sum_j^p k_{mij}[-m_{ij1} l_{ij1}(u_{xj} - u_{xi}) - m_{ij1}^2 (u_{zj} - u_{zi})]\Big\}. \quad (4)$$

To deduce the displacements accelerations, $\ddot{u}_{xi}$, $\ddot{u}_{yi}$ and $\ddot{u}_{zi}$, however, the spring constants between spheres i and j along the two tangential directions and the normal direction must be obtained firstly.

According to corresponding study,[19,20] the two tangential directions k_s, k_m and the normal direction k_n can be deduced by comparing the average strain energy in different ways after the arrangement patterns of spheres are determined.

Consequently, $[\ddot{u}_{xi}]_t$, $[\ddot{u}_{yi}]_t$ and $[\ddot{u}_{zi}]_t$ can be given by Eq. (4), where the symbol $[\ ]_t$ expresses the physical quantity at the moment t, the velocities of element i in the x, y, z directions $[\dot{u}_{xi}]_{t+\Delta t}$, $[\dot{u}_{yi}]_{t+\Delta t}$ and $[\dot{u}_{zi}]_{t+\Delta t}$ as well as the displacements $[u_{xi}]_{t+\Delta t}$, $[u_{yi}]_{t+\Delta t}$ and $[u_{zi}]_{t+\Delta t}$ can be obtained by Euler formula,

$$\begin{aligned}
[\dot{u}_{xi}]_{t+\Delta t} &= [\dot{u}_{xi}]_t + [\ddot{u}_{xi}]_t\,\Delta t,\\
[\dot{u}_{yi}]_{t+\Delta t} &= [\dot{u}_{yi}]_t + [\ddot{u}_{yi}]_t\,\Delta t,\\
[\dot{u}_{zi}]_{t+\Delta t} &= [\dot{u}_{zi}]_t + [\ddot{u}_{zi}]_t\,\Delta t,\\
[u_{xi}]_{t+\Delta t} &= [u_{xi}]_t + [\dot{u}_{xi}]_t\,\Delta t,\\
[u_{yi}]_{t+\Delta t} &= [u_{yi}]_t + [\dot{u}_{yi}]_t\,\Delta t,\\
[u_{zi}]_{t+\Delta t} &= [u_{zi}]_t + [\dot{u}_{zi}]_t\,\Delta t.
\end{aligned} \quad (5)$$

In Eq. (5), Δt represents a time increment. As is demonstrated, the DEM scheme can obtain related problems by following such process.

Generally, the tensile strength for many brittle materials such as glass is much lower than its compressive strength. The sample which is subjected to the tensile load would come to lose efficacy when the maximum principal stress reaches a critical point. We allege it as the failure criterion based on the maximum principal stress. The formula is

$$\sigma_1 < \sigma_\mathrm{b}, \quad (6)$$

where σ_1 is the first principle stress. σ_b is the maximum tensile stress.

Applied to the DEM model, the failure criterion expressed by essential parameter of DEM is proposed as follow

$$f_\mathrm{n} = \sigma_1 S < \sigma_\mathrm{b} S = f_\mathrm{b}, \quad (7)$$

in Eq. (7), S is operation area of the stress on a single element. f_n and f_b are the normal force and the tensile strength between two elements, respectively. However, the failure criterion between related elements is not equivalent to the failure criterion of samples, because there are several links from different directions focus on each element.

To verify the application of the DEM scheme on dynamic split of brittle material, we simulated the tension failure process of glass material composing ZnS by numerical method and compared the failure pattern with experiments.

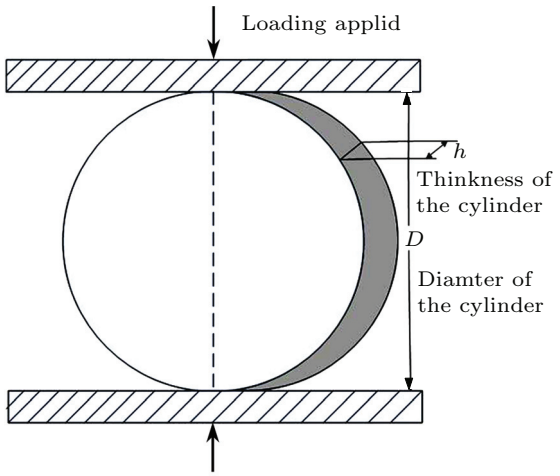

Fig. 2. The sketch of dynamic split test.

As shown in Fig. 2, a cylinder sample (length diameter ratio 0.5–1) is clamped between two press heads under the symmetrical load p which is go through center of the section vertically.[12] The dimension of the cylinder sample is 14.5 mm × 8 mm (diameter × thickness). The material parameters are: the mass density $\rho = 4\,090$ kg/m^3, the Young's modulus $E = 74.5$ GPa, and the Poison's ratio $\nu = 0.28$.

According to the static analytical solution of elastic mechanics, we can work out the stress of anywhere of the cylinder. Neglecting the influences of the stress concentration, the stress on the line of loading (except the nearby of force points) is obtained via the analytical solution,

$$\begin{aligned}
\sigma_x &= \frac{2P}{\pi h D},\\
\sigma_y &= \frac{2P}{\pi h D}\left(1 - \frac{4D^2}{D^2 - 4y^2}\right),\\
\tau_{xy} &= 0,
\end{aligned} \quad (8)$$

where, D is the diameter of the cylinder sample. h is the thickness of the cylinder, while P is the concentrated force, y is the ordinate of Cartesian coordinate system whose original point is center of the section O.

Furthermore, we can ignore the stress concentration supposing the fissure comes from the center point, and the tensile strength can be obtained

$$\sigma_\mathrm{t} = \frac{2P_\mathrm{max}}{\pi h D}, \quad (9)$$

where P_max is the maximum load.

In Eq. (9) the tensile stress in horizontal direction is equivalent. Moreover, the maximum of the compressive stress, which is $6P/\pi hD$, lies on the center of the disc, and the value is almost triple of the tensile coordinately. Regarding glass material, the compressive

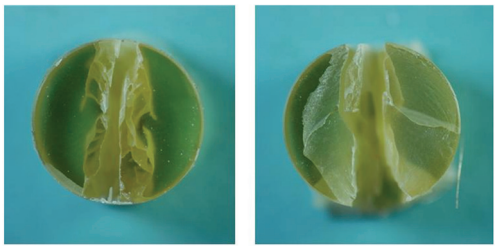

(a) (b)

Fig. 3. Two typical crack modes of the dynamic split by experiments.

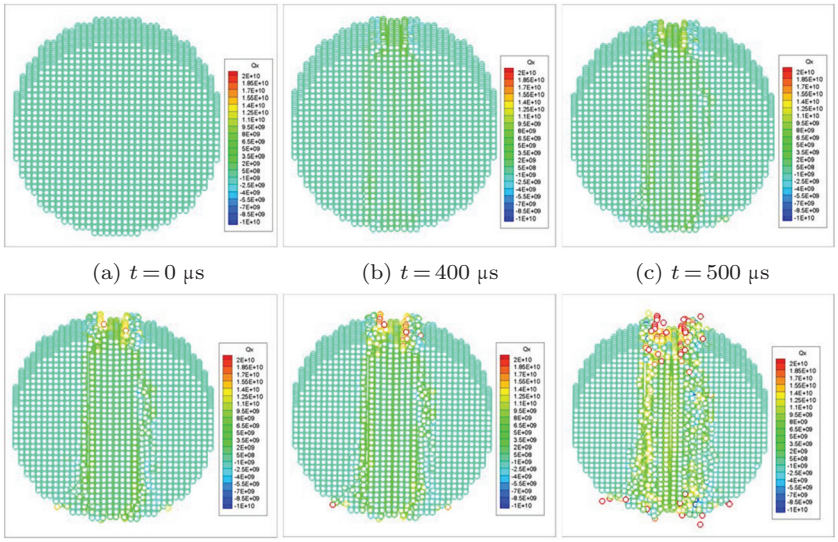

(a) $t = 0$ μs (b) $t = 400$ μs (c) $t = 500$ μs

(d) $t = 800$ μs (e) $t = 1\,000$ μs (f) $t = 1\,600$ μs

Fig. 4. The horizontal stresses σ_y from $t = 0$ μs to $t = 1\,600$ μs under the narrow load.

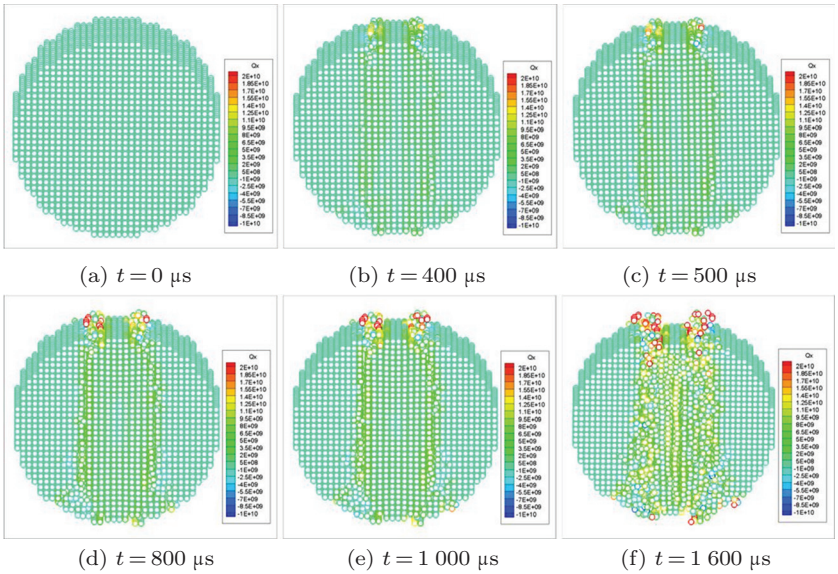

(a) $t = 0$ μs (b) $t = 400$ μs (c) $t = 500$ μs

(d) $t = 800$ μs (e) $t = 1\,000$ μs (f) $t = 1\,600$ μs

Fig. 5. The horizontal stresses σ_y from $t = 0$ μs to $t = 1\,600$ μs under the broad load.

strength is extremely higher than the tensile strength. Therefore, the sample is supposed to be damaged by the tensile stress instead of the compressive stress, and the crack is supposed to propagate along the vertical diameter of the cylinder theoretically. The discussion above is in allusion to the static situation. However, the dynamic tension of brittle glass is more difficult to describe, and also the fracture modes between dynamic split and static one differ from each other.

In order to carry out the tensile strength of this kind of specific glass, a series of dynamic splitting tests by using SHPB is conducted, and two typical fracture modes of the experimental results are shown in Fig. 3. The path of crack basically accords with the theory that is along the vertical diameter. However, by observing the transparent surface of samples, there are two other cracks on both sides of the centre one, but the two cracks that started from both sides of the cylinder have not connected with each other before the sample damaged in Fig. 3(a). And another sample crack snakes along other path in Fig. 3(b). That means the realistic failure mode of the dynamic split will be a band of crack. In order to analyze this phenomenon, we conducted several groups of numerical simulations by DEM.

For DEM simulation, models for 3-D problems are conducted to reproduce the damage processes, and the elastic constitutive relationship is applied in allusion to the brittle materials. Correspondingly, Fig. 4 shows the numerical results of horizontal stresses at time $t = 0$–$1\,600$ μs calculated by 3-D model (under the loading rate about 10 mm/min), which shows that the maximum appears at the centre area. According to Fig. 4(b), the maximum stress appears at the centre areas of the sample and the stress concentration area. In Fig. 4(c), we can find two yellow lines which represent the path of larger tensile stresses to appear from the edge of the speed-fixed elements. And then along with the spread of the stress wave, many elements along the path break and produce new crack as shown in Figs. 4(d) and 4(f). Finally it splits along the loading extension cord or the crack concentration area as shown in Figs. 4(e) and 4(f). It is worth mentioning that two elements on the top row of the model are added the fixed speed of 10 mm/min so as to simulate the distributing force.

To further confirm the influence of loading area and where cracks generate, we conducted a series of numerical simulations whose loading area vary from 2 mm to 6 mm. Taking the horizontal tensile stresses whose loading width are 6 mm as examples in Fig. 5, the regions appeared cracks has broadened obviously, and so as the paths of larger tensile stresses. By comparison, we confirm that the loading area of experiments would influence the crack mode of dynamic split distinctly. The broader the loading region is, the larger the crack band would be under the same loading rate. Consequently, to obtain the accurate centre crack deduced by classical theory and eliminate the interference of crack band, the great effort should be done on narrowing the loading area.

Based on both experiments and numerical simulations by DEM, we propose the reason is that the loads on the samples are distributing forces instead of concentrating ones. To avoid slipping during experiments, the both edges of samples need to be rubbed down slightly. Consequently, there are two stress concentration fields on each edge of the loading area.

As shown in Figs. 4(b) and 4(c), we can see that, in the area where cracks may accrue firstly. It is not only suffered the tensile stress, but also the relative slippage in the y condition on the edge of the load. Therefore, the type of cracks should be the I–II mixed mode. While loading applied, the strain energy in the stress concentration area around the edge of load attains its maximum, and enough energy accumulates. Then the mixed mode cracks snake from both two sides of the sample along the direction of the maximum energy release rate (see Fig. 4(c)). However, the opened crack, which is basically along the vertical diameter and started from centre area, will appear later when the tensile stress is large enough, as shown in Fig. 4(e). The sample may damage basically along the vertical diameter if the centre crack has spread to both sides of the sample before the mixed cracks connected. On the other hand, it also may split along other way within the crack band if mixed mode cracks snake faster.

In this work, the fracturing damage process of the dynamic split experiment of a special brittle glass ZnS is investigated numerically and experimentally. It is proved that the crack modes of dynamic split are different from those of static split, the practical conditions of dynamic split experiments would result in a crack band which is different from the classical theory. Moreover, the formation process of the crack band is investigated. The width of the crack band is determined by the width of loading area.

This work was supported by the National Natural Science Foundation of China (10732010, 10972010 and 11028206).

1. Q. Z. Wang, and F. Feng, Engineering Fracture Mechanics **78**, 2455 (2011).
2. S. H. Chang, and C. I. Lee, Engng. Geol. **66**, 79 (2002).
3. M. R. Ayatollahi, and M. R. M. Aliha, Int. J. Rock. Mech. Min. Sci. **44**, 617 (2006).
4. H. Kolsky, Proc. Roy. Soc. Lon. B **62**, 676 (1949).
5. J. W. Tedesco, and C. A. Ross, Computers & Structures **32**, 609 (1989).
6. H. Zhao, and G. Gary, Int. J. Solids Structures **33**, 3363 (1996).
7. D. E. Lambert, and C. A. Ross, International Journal of Impact Engineering **24**, 985 (2000).
8. J. W. Tedesco, and M. L. Hughes, Computers & Structures **51**, 65 (1994).
9. J. Rodríuez, and V. Sáchez-Gávez, Journal de Physique **4**, c8101 (1994) (in Germany).
10. R. D. Adams, and J. A Harris, Int. J. Adhes. **16**, 61 (1996).
11. A. M. Bragov, and A. K Lomunov, Int. J. Impact. Energy **16**, 321 (1994).
12. O. S. Lee, and S. S. Lee, KSME Int. J. **12**, 1143 (1998).

13. P. A. Cundall, and D. O. Potyondy, Geotechnique, **29**, 47 (1979).
14. K. Tadahiko, and K. Yasuhiro, J. Seisan Kenkyu **29**, 288 (1977).
15. Y. Sawamoto, and H. Tsubota, Nucl. Eng. Des. **179**, 157 (1998).
16. K. X. Liu, and L. T. Gao, Acta Mech. Sol. **16**, 256 (2003).
17. K. X. Liu, and L. T. Gao, JSME Int. J. Ser. A **47**, 138 (2004).
18. K. X. Liu, and W. F. Liu, Appl. Mech. **76**, 229 (2006).
19. L. Shan, and K. X. Liu, Chin. Phys. Lett. **26**, 120202 (2009).
20. M. Cheng, and K. X. Liu, Acta Mech. Sin. **25**, 629 (2009).